Applied Catalysis B: Environmental 96 (2010) 569–576

Contents lists available at ScienceDirect

Applied Catalysis B: Environmental

journal homepage: www.elsevier.com/locate/apcatb

The effect of particle shape on the activity of nanocrystalline TiO_2 photocatalysts in phenol decomposition. Part 2: The key synthesis parameters influencing the particle shape and activity

Nándor Balázs, Dávid F. Srankó, András Dombi, Pál Sipos, Károly Mogyorósi *

Department of Inorganic and Analytical Chemistry, University of Szeged, Research Group of Environmental Chemistry, Szeged, H-6701, P.O. Box 440, Hungary

ARTICLE INFO

Article history:
Received 25 November 2009
Received in revised form 1 March 2010
Accepted 3 March 2010
Available online 9 March 2010

Keywords:
Titania
Anatase
Rutile
Nanoparticles
Phenol decomposition
Photocatalysis
Flame hydrolysis
Shape dependence

ABSTRACT

Nanosized TiO_2 photocatalysts were synthesized via hydrogen–air flame hydrolysis by using two slightly different, home made diffusion flame burners (Burners A and B). Titanium(IV) chloride vapor was introduced into the flame via bubbling dry air throughout the precursor liquid. X-ray diffraction (XRD) measurements revealed that the particles are anatase–rutile mixtures with a phase composition ranging from 98:2 to 57:43 anatase to rutile weight ratio. The hydrogen–oxygen molar ratio in the flame, as well as the precursor vapor feeding rate were found to be the key parameters which determine both particle structure and morphology. Spherical and polyhedral particles with significantly varying photocatalytic activity were produced in Burner A by increasing the precursor vapor feeding rate at a constant hydrogen–oxygen molar ratio, the photocatalytic activity increased for samples synthesized. The differences in particle size, specific surface area and anatase–rutile composition were found to be marginal but the particle shape changed from spherical to polyhedral by increasing that parameter. From this, it was concluded that particle shape plays an important role in photocatalytic activity, the faceted particles are better photocatalysts than spherical ones. With Burner B, predominantly polyhedral particles were obtained, some of them with further improved photocatalytic activity. Synthesis parameters for obtaining maximum activity have been established for both burners. Our results prove, that bare (undoped) TiO_2 photocatalysts with photocatalytic activity significantly better than that of P25 can routinely be prepared and their performance optimized via the fine-tuning of the synthesis parameters employed.

1. Introduction

In our recent publication [1], titanium dioxide nanoparticles prepared via flame hydrolysis method were systematically investigated for the photocatalytic decomposition of model compounds, such as phenol in aqueous solution and methanol or acetaldehyde in gas phase. It was demonstrated that the photocatalytic performance varied by the systematic change of the crystal shape. Polyhedral particles were found to be more efficient than spherical ones for the decomposition of phenol and methanol. The important synthesis parameters influencing the crystal shape were not described earlier; this is one of the primary goals of the present paper.

Since the photocatalytic performance depends on several structural parameters, it is very important to well control as many of them as possible. Among these, the most crucial parameters are the crystal phase [2], particle size (specific surface area) [3] and the surface properties of the photocatalysts. Ryu and Choi found that the photocatalytic activity of a given photocatalyst also depends on the model substrate used for testing [4]. Among the commercial photocatalysts studied, Degussa P25 TiO_2 (P25 in the followings) was found to display the best photocatalytic activity for the majority of the organic compounds investigated. Well adsorbing molecules, like carboxylic acids, were found to decompose slowly, while ill-adsorbing compounds are all relatively rapidly oxidized in the presence of UV-irradiated P25 [5–7]. Since P25 photocatalyst is made by flame hydrolysis, it brings up the idea to study this synthesis method in details and to further improve it in order to produce both bare and doped titania photocatalysts with further improved photocatalytic activity. Although that commercial titania is widely accepted as one of the best available photocatalysts, frequently chosen to be as a reference, there are still not too many papers in which material and photocatalytic properties of samples made by similar methods would have been studied systematically [8–20]. Many authors optimizing the synthesis parameters for controlling the particle size and phase composition did not study the photocatalytic properties of their products at the same time [21–35]; this is because, titanium dioxide, besides photocatalysis has many

* Corresponding author. Tel.: +36 62 544 338; fax: +36 62 420 505.
E-mail address: k.mogyorosi@chem.u-szeged.hu (K. Mogyorósi).

0926-3373/$ – see front matter © 2010 Elsevier B.V. All rights reserved.
doi:10.1016/j.apcatb.2010.03.006

other applications, for example in paintings, pigments and filling substances.

Flame made titania nanoparticles are typically produced in a process which involves the introduction of the titanium(IV) precursor into the flame as its vapor or very small droplets. In the first method, an inert carrier gas is bubbled through the liquid precursor which transports the molecules into the high temperature flame zone containing water molecules. The latter method is called flame spray method in which the droplets of the precursor or its solution are directly injected into the flame. The hydrolysis of the titanium precursor occurs in both cases that is followed by the very rapid crystallization of the nuclei thus formed. This results in highly crystalline titanium dioxide particles in an aerosol form which is finally trapped in a filter or a condenser. The titanium dioxide nanoparticles thus produced are mostly in the diameter range of 3–150 nm and the product is typically an anatase–rutile mixture. Authors used different flame configurations, different carrier (Ar, air, N_2), oxidant (O_2 and air) and fuel gases (CH_4, H_2), mixing them into the burner in different ratios and at different flow rates. This enabled the researchers to optimize the synthesis for a given goal (to obtain the desired particle size, phase composition or the highest photocatalytic activity).

In our studies, two slightly different diffusion flame burners were used to establish both the optimal hydrogen–oxygen molar ratio and the flow rate of titanium(IV) chloride vapor. The process parameters were tuned to receive the highest photocatalytic activity sample for phenol photocatalytic degradation. As it was demonstrated in our previous paper [1], samples with superior photocatalytic activity contained mostly polyhedral particles. Therefore, the synthesis parameters were also optimized to obtain mostly polyhedral particles in the products.

2. Experimental

2.1. Synthesis of the photocatalysts

Two burners of the home made co-flow diffusion flame reactors equipped with a bubble vapor generator are shown in Fig. 1 (Burners A and B). Both reactors consist of a central tube through which the precursor ($TiCl_4$, Fluka 99% purity) is fed into the flame via bubbling dry air through it. The flame is air-fed. The fuel (H_2) intake is made through seven capillaries (Burner A) and eight capillaries (Burner B) situated concentrically around the precursor vapor feeding tube in both burners. This way the air acts as oxidant and as the sheath gas (similarly to the design described in refs. [13,16,19,22,30]). Burner A is made of glass and the upper ~5.5 cm part of Burner B is made of quartz (the upper part is specially glued to the lower part which is made of glass) in order to provide better heat resistance. The inner diameter of the capillary tubes (1 mm), the hydrogen intake tubes (a = 5 mm) and the inner diameter of the vapor feeding tubes (b = 3 mm) are the same for both burners, but the external diameter of the two burners are different (c = 27 mm, d = 35 mm). This means also that the distance between the capillary tubes is larger for Burner B than for Burner A. There was a glass tube fitted onto the precursor vapor feeding tube in Burner A in order to make its cleaning easier. Burner B was made with a flexible (removable) precursor vapor feeding tube (its vertical position can be adjusted).

The experimentally accessible parameter range for the two burners was determined in preliminary experiments (in which stable flame was formed). For Burner A, the total flow rate of the air was changed between 5070 and 6400 mL/min and the hydrogen flow was kept constant (1230 mL/min) in order to set the desired hydrogen–oxygen molar ratio in the flame which was varied between 0.76 and 1.25. The flow rate of air bubbling through

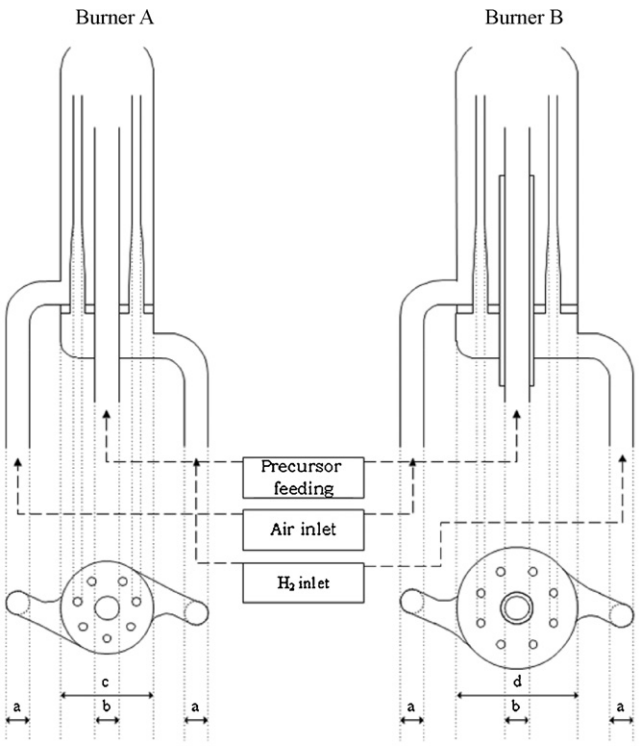

Fig. 1. Configuration scheme of Burner A and B.

the $TiCl_4$ was systematically changed from 118 to 355 mL/min (taken from the above mentioned total air flow). Since the geometry of Burner B is somewhat different from that of Burner A, stable flame can be created by using the following parameters for the latter: the total flow rate of the air was changed between 6420 and 7100 mL/min and the hydrogen flow was set to be at 1420–1810 mL/min keeping the total gas flow rate approximately constant (8230–8520 mL/min). The hydrogen–oxygen molar ratio was varied between 1.00 and 1.41 in the flame with this method. The flow rate of air bubbling through the $TiCl_4$ was systematically changed between 178 and 710 mL/min (splitted from the total air flow given above).

The flow rates were separately controlled with calibrated rotameters (Cole–Parmer). The TiO_2 aerosol was driven to a conical chimney, which drove the product to a water-cooled glass collector. For more details of the reactor, see in [1].

The particles were purified via using a Medicell dialysis sack (MWCO = 12–14,000 Da). The suspensions were dried at 120 °C and the powders were finally ground in an agate mortar.

In the names of the samples, the type of the burner, the hydrogen–oxygen molar ratio, the precursor vapor feeding rate in mL/min and the temperature of the liquid precursor under bubbling in °C are indicated; these parameters are separated by hyphens, for example: A-0.96-148-30.

2.2. Characterization of the photocatalysts

Sample characterization has been described in details in our previous publication [1]. X-ray diffraction (XRD) measurements were performed on a Rigaku diffractometer (MiniFlex II benchtop XRD system) (Cu Kα = 0.15406 nm, 40 kV, and 30 mA, in the $20^\circ \leq 2\Theta \leq 30^\circ$ regime). The average diameters of the particles were obtained by means of the Scherrer equation. In order to characterize the phase composition of the powders, the diffraction peaks were recorded and integrated. The samples contained anatase and rutile phase only. The weight fraction of anatase and rutile was calculated from the comparison of the integrated XRD-peak areas.

Transmission electron microscopic (TEM) studies were performed to characterize the particle size and size distribution and also to establish the predominant morphology of the particles. TEM micrographs were recorded on a Philips CM 10 instrument operating at 100 kV using Formvar coated copper grids.

The specific surface area of the catalysts was determined by nitrogen adsorption at 77 K by a Micromeritics gas adsorption analyzer (Gemini Type 2375). The specific surface area was calculated using the BET method.

2.3. Determination of the photocatalytic activities

The photocatalytic performance of the catalysts prepared was characterized by using the photocatalytic decomposition of phenol in aqueous solution. The photoreactor (100 mL) was an open tube with double walls, surrounded by a thermostating jacket ($25.0 \pm 0.1\,^{\circ}C$). The continuously stirred reactor was surrounded and irradiated by six fluorescent lamps (6 W power, radiation maximum at 365 nm, intensity of UV light was $I = 1.02 \pm 0.01 \times 10^{-6}$ einstein s^{-1} measured utilizing ferrioxalate actinometry). The concentration of phenol was measured with an HPLC system consisting of a Merck-Hitachi L-7100 low-pressure gradient pump equipped with a Merck-Hitachi L-4250 UV–VIS detector and a Lichrospher RP 18 column applying methanol/water mixture as eluent. Detection wavelength was set to 210 nm. The initial concentration of the substrate was 5.0×10^{-4} M. 1 g dm^{-3} photocatalyst concentration was used throughout. No adsorption of phenol was observed on the surface of TiO_2 specimens studied in this work, therefore the actual concentration of the substrate in the solution phase was regarded to be equal to the concentration of the unreacted phenol. Samples were taken from the suspension in predetermined time intervals, usually for 100–120 min. Further details on the experimental set-up have been described in details elsewhere [1–2].

The initial rate of the photocatalytic degradation of the model compounds, r_0 was considered to be the measure of the efficiency of a given photocatalyst. To determine r_0, an empirical function was fitted to the experimentally observed $c = f(t)$ data points at the conversion range of <60% (in some cases <80%). If the fitting yielded satisfactory description for the data then the slope of the empirical function at $t = 0$ yields the initial rate of the photocatalytic reaction.

3. Results and discussion

3.1. Characterization of the photocatalysts

The photocatalysts prepared via using Burners A and B were characterized by transmission electron microscopy. Representative samples from both series are presented in Table 1. The preparation conditions are listed here, such as hydrogen flow rate, air flow rate and their sum as total gas flow rate expressed in mL/min. The applied precursor vapor feeding rates are also shown for these samples. For each individual sample, the calculated hydrogen–oxygen molar ratio during preparation is also given in the name of the sample. TEM images of the most interesting photocatalysts are shown in Fig. 2.

Particles prepared in Burner A were mostly spherical ones when low precursor vapor feeding rate was applied (see Table 1. and Fig. 2.) For sample A-1.21-237-30 only spheres were observed. Keeping the hydrogen–oxygen molar ratio near to one, the particle shape can be fine tuned. In order to make this shape parameter numerically expressible [1], the following shape classifications were made: a particle was defined to be polyhedral, if it was seen to be terminated mostly by linear sections rather than by arcs on the TEM projection. Counting the number of polyhedral and spherical particles for the given sample, the frequency of polyhedral particles in percentage of the total number of particles was expressed. The frequency of polyhedral particles could have been increased between 10% and 69% simply by changing the precursor vapor feeding rate from 148 to 355 mL/min. Samples prepared by using Burner A (Table 1.) are identical to the samples listed in our previous publication (i.e., [1], Table 1, sample nos. 1, 2, 4, 5 and 8). When the flame synthesis reactor was tested for preparing doped TiO_2, the aperture of the precursor vapor feeding tube in Burner A was accidentally narrowed by the deposition of a thermally decomposed doping precursor. This irreversible change in the inner diameter of the precursor vapor feeding tube led us to the observation, that this parameter also influences the shape of the particles synthesized. The synthesis of sample A-0.96-355-30 was repeated with the narrowed precursor vapor feeding tube and we found 99% frequency of the polyhedral particles in that sample instead of 69% (this sample was presented as sample no. 9 in our previous publication [1]).

Knowing that, we designed Burner B in which such an irreversible change can simply be avoided since the precursor vapor feeding tube is removable and its vertical position is adjustable. This also makes the inner diameter a further variable parameter in our burner. The synthesis parameters of samples prepared in Burner B are also listed in Table 1. There are only six selected samples listed here from series B. The first three samples were chosen from a series in which the hydrogen–oxygen molar ratio was changed between 1.00 and 1.41, holding the other parameters essentially unchanged (total gas flow rate was between 8230 and 8520 mL/min, in average 8375 ± 145 mL/min, ±2%; the precursor vapor feeding rate was 355 mL/min). The next two samples (B-1.24-178-30 and B-1.24-710-30) were selected from a series in which the flow rate of hydrogen and air was constant (1680 and 6760 mL/min, respectively) and therefore the total gas flow rate was also constant (8440 mL/min), but the precursor vapor feeding rate varied between 178 and 710 mL/min. All these samples were made via keeping the temperature of the precursor liquid to $30.0 \pm 0.2\,^{\circ}C$. A further sample (B-1.24-355-70) was selected from a series in which the temperature of the liquid titanium(IV) precursor was changed between 30 and 70 °C and the hydrogen, the air flow rate and the precursor vapor feeding rate were kept constant (1680, 6760 and 355 mL/min, respectively). As it can be seen from the data presented, the shape analysis resulted in 90–100% for the frequency of polyhedral particles for all the samples made by Burner B. There are only minor differences among these particles comparing their shape classification. Their size analysis results will be discussed later.

It was stated earlier that there are different P25 qualities in use at different research groups. In our studies we investigated two different qualities, using the same names as in our previous paper such as P25 A and B, which are different in the anatase-rutile weight ratio (79:21 and 89:11, respectively) and also in their photocatalytic activity. P25 B reference is also commercially named as Aeroxide P25 TiO_2.

XRD patterns of the selected samples in Table 1 are shown in Fig. 3. It is obvious from the position of the diffraction peaks that these products contain mostly anatase particles (peak at 2Θ = 25.3°,) and some rutile (2Θ = 27.5°,). The weight fraction of anatase and rutile can be calculated directly from the peak area values [36]. This calculation revealed, that the TiO_2 samples thus prepared consisted mainly of anatase (80–97 wt%) and the rest is rutile. Unusually high rutile content (43 wt%) was found for sample B-1.41-355-30. Comparing the XRD patterns of the three selected samples for which the hydrogen–oxygen molar ratio varied as 1.00-1.24-1.41, it can be concluded that the increasing hydrogen–oxygen molar ratio promoted the formation of particles with rutile phase (4, 18 and 43 wt%, respectively). This can be due to the higher flame temperature caused by the higher fuel concentration [19], which

Table 1
Synthesis parameters used for preparing nanocrystalline TiO_2 photocatalysts, employing Burner A and B and the frequency of the polyhedral particles in the specimens.

Sample	H_2 flow rate (mL/min)	Air flow rate (mL/min)	Total gas flow rate (mL/min)	Precursor vapor feeding rate (mL/min)	Frequency of polyhedral particles (%)
A-1.21-237-30	1230	4850	6080	237	0
A-0.96-148-30	1230	6100	7330	148	10
A-0.96-178-30	1230	6100	7330	178	33
A-0.96-237-30	1230	6100	7330	237	59
A-0.96-355-30	1230	6100	7330	355	69
B-1.00-355-30	1420	7100	8520	355	100
B-1.24-355-30	1680	6760	8440	355	96
B-1.41-355-30	1810	6420	8230	355	90
B-1.24-178-30	1680	6760	8440	178	95
B-1.24-710-30	1680	6760	8440	710	97
B-1.24-355-70	1680	6760	8440	355	97
P25 B	–	–	–	–	100

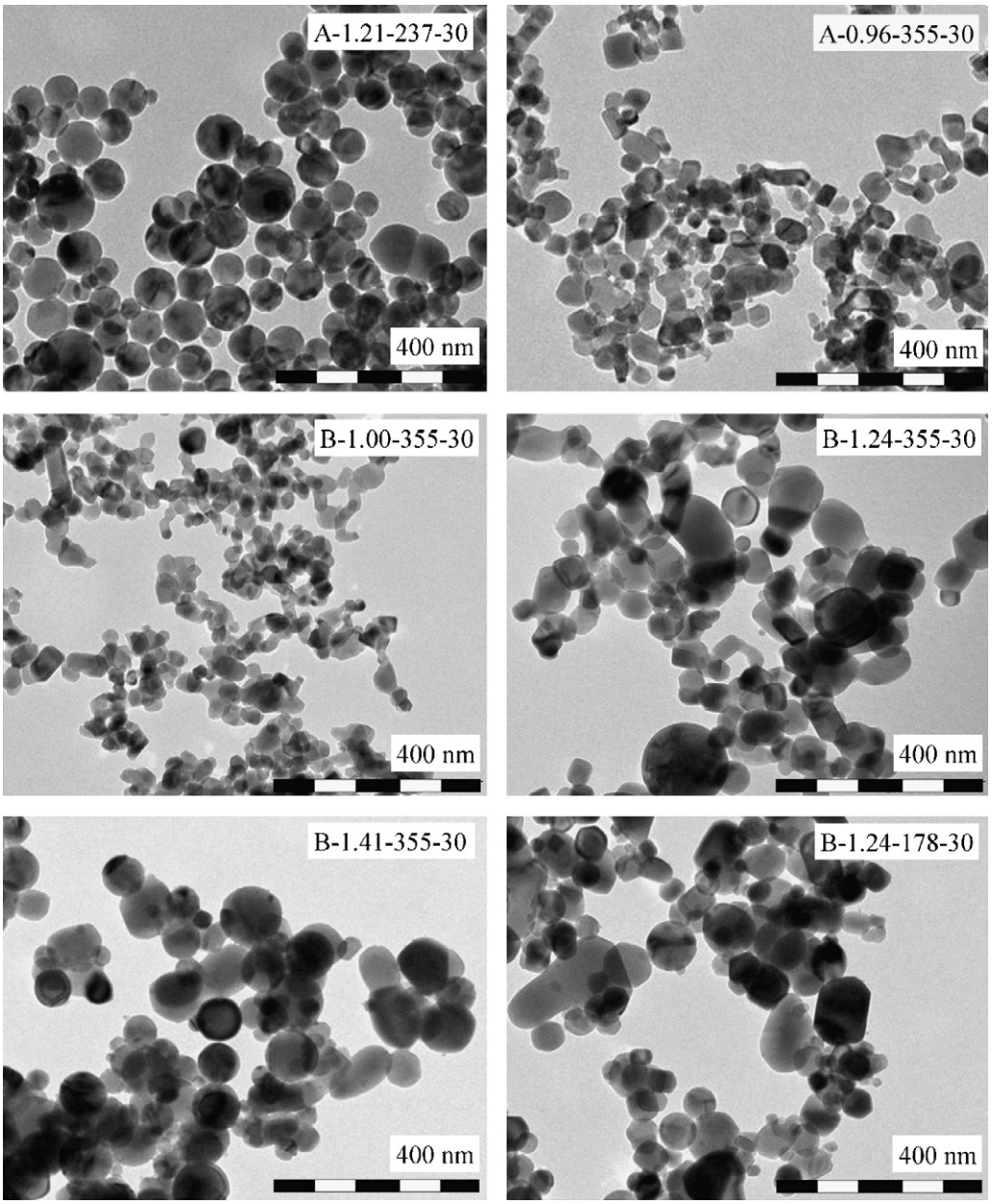

Fig. 2. TEM images of selected samples prepared in Burner A and Burner B. For specimen annotation, see text. Both spherical and polyhedral particles are seen for samples A-1.21-237-30 and A-0.96-355-30, made by Burner A, while particle morphology is predominantly polyhedral for samples made in Burner B.

causes anatase–rutile phase transformation or due to the presence of titanium(III) at higher density in the crystal lattice which can also accelerate the formation of the rutile phase [25]. The anatase and rutile particle size of these materials were estimated from the line broadening of the given peaks by the use of Scherrer equation. It should be noted however that these values are not very accurate since these particles are too large (>40 nm) for such a determination (therefore the line broadening effect is too small).

3.2. Photocatalytic performance of the samples

The photocatalytic activities of the samples were determined under UV irradiation using phenol as model substrate. Selected decay curves are presented in Fig. 4, i.e., for the highest and lowest activity samples from both series A and B. The fitted curves by using an empirical function up to 60% conversion are also shown in Fig. 4. The photocatalytic activity of P25 A and B can be directly compared with these samples. Significantly higher activities were found for samples prepared in both burners under specified synthesis conditions. The representative structural parameters are listed for the most interesting samples in Table 2. Besides the frequency of polyhedral particles and anatase to rutile ratio, the specific surface area of the samples, the calculated average particle diameters from TEM measurements and the initial decomposition rates of phenol (r_0) are given in Table 2.

On the basis of the structural parameters of these specimens, the most interesting observation is that although the structural properties of the particles prepared by Burner A are just slightly different, major variations are seen in their photocatalytic activity. For example, the specific surface are values varied between 20 and 28 m^2/g, the particle diameters were in the range of 51–63 nm and the anatase to rutile weight ratio changed between 98:2 and 89:11. These are marginal differences but at the same time the photocatalytic decomposition rate for phenol varied between 7.2 and 20.2 $M\,s^{-1}$. Such a significant enhancement in photocatalytic activity cannot be attributed to any traditionally investigated simple structural property. Although we were not able to find any obvious systematic variation among these properties, it was recognized that our particles made by Burner A are interestingly different in their shapes. Our TEM measurements demonstrated that in the less active catalysts the dominant morphology of the particles is spherical, while polyhedral (cubic or hexagonal) shapes predominate in the samples with superior photocatalytic activity (see Fig. 2.) This is easily noticeable if we place the TEM images of sample A-1.21-237-30 and sample A-0.96-355-30 next to each other. It is rather important to note that simply by increasing the precursor vapor feeding rate the particle shape can be focused on having more polyhedral particles and higher photocatalytic activity at the same time (while keeping the hydrogen–oxygen molar ratio constant, 0.96).

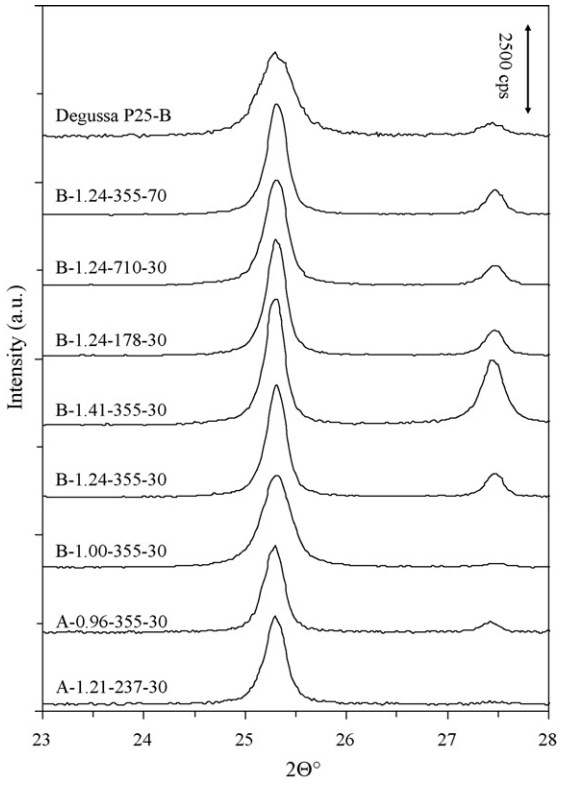

Fig. 3. X-ray diffraction patterns of selected samples from series made by Burner A and B. For specimen annotation, see text. Anatase and rutile reflections are seen at $2\Theta = 25.7°$ and 27.8°, respectively.

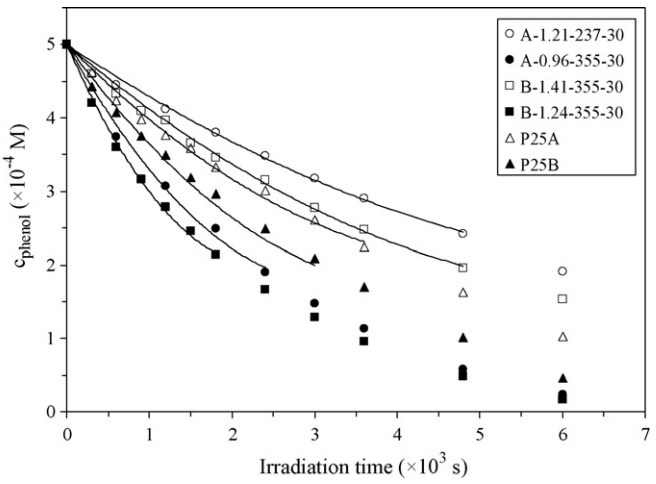

Fig. 4. Phenol photocatalytic decomposition curves at $c_{0,phenol} = 0.5$ mM and $c_{TiO_2} = 1.0$ g/L, via using the samples with the highest and lowest photocatalytic activity, prepared with Burner A and B. For specimen annotation, see text. For comparison, decay curves obtained for Degussa P25 A and B are also shown.

Upon recognizing the technical problems associated with the fixed inner tube in Burner A, Burner B was designed. Naturally we also considered other disadvantages of Burner A in order to make Burner B more suitable for producing larger quantities of high activity photocatalysts. These led us to the changes between the two burners described earlier. At the same time this also makes the comparison of the two burners possible providing the same flame configuration but somewhat different geometry. One could expect that this will not cause major variations in the material properties. However, it was found, that using Burner B and varying the same key parameters (hydrogen–oxygen molar ratio and then the precursor vapor feeding rate) mostly polyhedral particles were formed only (usually from 90% to 100%). For series A and B, the optimization of the use of the burners was studied varying first the hydrogen–oxygen molar ratio and then – keeping that individual optimal parameter – the optimal hydrogen–oxygen molar ratio was determined. Fig. 5a and b demonstrates how these parameters influence the photocatalytic activity and the anatase content in the samples made in Burner A. It is obvious from Fig. 5a that the optimum of the applied hydrogen–oxygen molar ratio is near to 1 (the flow rate of the precursor vapor was 237 mL/min). Increasing the concentration of the fuel in the gas mixture combusted, the anatase content remained almost unchanged (it increased from 91 to 94 wt% only). It is to be noted here, that the empty and full symbols represent the given data belonging to two individually prepared (that is: independently reproduced) samples. Two full symbols are at the same synthesis parameter indicated if the

Table 2
Structural data and photocatalytic activity of nanocrystalline flame synthesized TiO_2 photocatalysts, made by using Burner A and B. For specimen annotation, see text.

Sample	Frequency of polyhedral particles (%)	Anatase to rutile ratio	Specific surface area ($m^2\ g^{-1}$)	Average particle diameter from TEM (nm)	Initial reaction rate (10^{-8} M s^{-1})	Initial reaction rate/(specific surface area × catalyst loading) (10^{-9} mol s^{-1} m^{-2})
A-1.21-237-30	0	97: 3	25	63	7.2	2.9
A-0.96-148-30	10	96: 4	20	60	10.9	5.5
A-0.96-178-30	33	98: 2	24	62	11.3	4.7
A-0.96-237-30	59	92: 8	28	51	15.9	5.7
A-0.96-355-30	69	89: 11	27	55	20.2	7.5
B-1.00-355-30	100	96: 4	45	38	14.7	3.3
B-1.24-355-30	96	82: 18	21	69	25.7	12.2
B-1.41-355-30	90	57: 43	19	77	9.8	5.2
B-1.24-178-30	95	80: 20	24	61	21.4	8.9
B-1.24-710-30	97	84: 16	27	59	20.4	7.6
B-1.24-355-70	97	81: 19	22	72	19.4	8.8
P25 B	100	89: 11	50	26	15.4	3.1

measurement was repeated for the same sample. This way the reproducibility of the synthesis and the characterization of the materials can be separately studied. Fig. 5b reveals that the photocatalytic activity was the highest if the highest precursor vapor feeding rate was applied (keeping the hydrogen–oxygen molar ratio at 0.96). This parameter could have not been further increased due to technical limitations in Burner A, due to the fluctuations of precursor mass flow. The anatase content of the powders gradually decreased in a relatively narrow range (between 95 and 85 wt%). It is possible that introducing more $TiCl_4$ resulted in higher temperature in the flame due to its reaction is exothermic. Fig. 5c shows the hydrogen–oxygen molar ratio dependency on the photocatalytic activity and on the anatase content of the materials produced in Burner B. Similar systematic variation was observed for Burner A, except that the maximum is here about 1.25. However the anatase content decreased by increasing the concentration

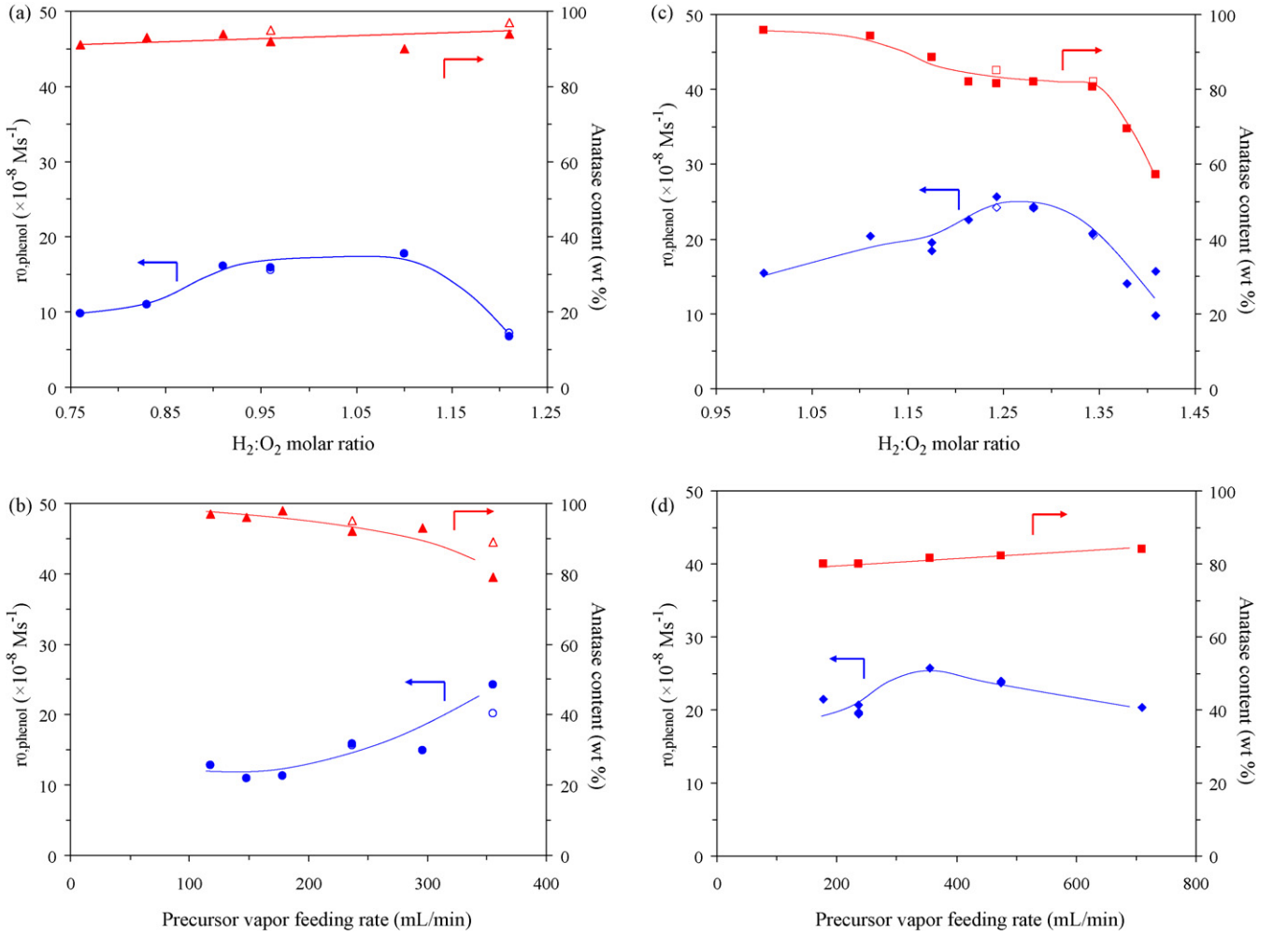

Fig. 5. (a and b) dependence of the photocatalytic activity and the anatase content of products by using Burner A; (a) effect of varying the hydrogen–oxygen molar ratio at constant precursor vapor feeding rate (270 mL/min); (b) effect of varying the precursor vapor feeding rate at constant hydrogen–oxygen molar ratio (0.96); (c and d) dependence of the photocatalytic activity and the anatase content of products by using Burner B; (c) effect of varying the hydrogen–oxygen molar ratio at constant precursor vapor feeding rate (355 mL/min); (d) effect of varying the precursor vapor feeding rate at constant hydrogen–oxygen molar ratio (1.24).

of the fuel, this change became more pronounced above 1.35. It should be noted here that the presence of more hydrogen resulted in somewhat reducing environment, for samples prepared at the two highest hydrogen–oxygen molar ratio an obvious blue color appeared indicating the presence of Ti(III) in the crystal lattice. Keeping this parameter constant near to the maximum (1.24), the precursor vapor feeding rate was also optimized. Fig. 5d shows that there is a maximum at about 355 mL/min for samples prepared in Burner B. Comparing Fig. 5b and d, an opposite trend can be found for the anatase content of samples prepared in the two burners. For the latter case, the anatase content slightly but systematically increased from 80 to 84 wt%. It is hard to make a conclusion why these parameters affected the anatase content in one way or in the other. It is obvious though that keeping the precursor vapor feeding rate constant, the rutile content can be fine tuned simply by changing the amount of hydrogen introduced into the flame in the case of Burner B. Varying that parameter, the particle diameter also increased significantly (from about 40 to 80 nm). This makes the assumption more plausible that higher temperature was reached at higher hydrogen content which resulted in the anatase–rutile phase transformation and the sintering (growing) of these particles.

It is interesting to note that many photocatalysts prepared by us showed higher activity than P25 B. Our sample named B-1.00-355-30 is very similar to P25 B: their particle diameter, specific surface area, the frequency of polyhedral particles and the photocatalytic activity are practically identical (see Table 2). The only significant difference is seen in their rutile content (instead of 21 wt% it is only 4 wt%). P25 A and B are different in their anatase to rutile ratio (79:21 and 89:11, respectively) and their photocatalytic activities are also somewhat different ($r_{0,\text{phenol}}$ is 11.8 and 15.4×10^{-8} M s^{-1}, respectively). In their case the higher anatase content was accompanied with higher photocatalytic activity. Our HRTEM images published in our previous paper [1] demonstrated that the rutile and anatase particles in our samples exist as individual single crystals, and not as interwoven rutile–anatase composites as it was claimed [37,38] (but not confirmed by others [39]) for P25. We concluded that the rutile content might not play such an important role in the very high photocatalytic activity of flame made TiO_2 samples, as it was thought by researchers considering a so-called "antenna" effect [37,38]. The data presented in this paper confirmed that the highest photocatalytic activity can be found for samples with relatively large particle diameters and relatively low specific surface areas (50–70 nm and 20–28 m^2/g, respectively). The highest activity samples were produced under the described optimal synthesis conditions yielding mostly polyhedral particles for which the typical anatase content is between 80 and 90 wt%.

Calculating the rate of photocatalytic reaction normalized with the surface area (i.e., dividing $r_{0,\text{phenol}}$ by $a^S_{BET} \times$ photocatalyst loading, yielding $r_{0,\text{phenol}}$' in Table 2), an interesting comparison can be made. The highest $r_{0,\text{phenol}}$' were found for sample A-0.96-355-30 (7.5×10^{-9} mol s^{-1} m^{-2} from series A) and for sample B-1.24-355-30 (12.2×10^{-9} mol s^{-1} m^{-2}, from series B). These values are significantly higher than those determined for P25 A and B (2.4 and 3.1×10^{-9} mol s^{-1} m^{-2}, respectively). In our opinion this demonstrates, that the highest photocatalytic activity expressed over the surface unit exists when relatively large nanoparticles are formed with well-crystallized form in faceted surface structure. This is an important statement if we consider that on the basis of the open literature, flame synthesis procedures produced almost exclusively spherical titania particles [13,16,18,20,21,27,29,35,40–43] and oblong shaped nanocrystals were observed only in a few instances [27,30,31,33,34]. Sol–gel syntheses yielding polyhedral or non-spherical (such as cuboid [44], hexagonal [45] and rod-like [46]) TiO_2 nanoparticles are well known from the literature but to the best of our knowledge, there is no systematic comparison of the photocatalytic activity of polyhedral and spherical particles owning very similar structural parameters in these publications.

Naturally many other structural parameters could influence the photocatalytic activity, such as the hydrophilicity of the surface [26], the substrate and oxygen adsorption properties of the photocatalysts [2,4,47] and also the crystal face dependent number (or density) of recombination centres or the anisotropic charge transport in TiO_2 [48]. In the third part of this series, we further extend our studies on the material properties of these photocatalysts. Hydrophilicity of the particles is characterized by dynamic light scattering measurements in suspensions, special surface properties are determined by XPS technique, oxygen consumption experiments in irradiated suspensions, intermediate analysis and TOC measurements are used to study the mechanism of the complete mineralization of phenol on the different flame made titanias. This complete characterization provides a better understanding on the overall material properties and the efficiency of such prepared photocatalysts.

4. Conclusions

Titanium dioxide photocatalysts have been prepared in flame synthesis in hydrogen–air flame using titanium(IV) chloride as a precursor, and via employing two slightly different, vapor fed burners. It has been established, that the photocatalytic activity of the products thus obtained can be maximized via systematically varying the hydrogen–oxygen molar ratio in the flame and the precursor vapor feeding rate. Besides the most plausible structural parameters (i.e., particle size, specific surface area and phase composition); the shape of the nanoparticles was found also to be a key parameter affecting the activity. Owning similar material properties in the end product, the particle shape could have been changed from spherical to polyhedral simply by changing the precursor vapor feeding rate in Burner A. Burner B produced mostly polyhedral particles under all conditions. The optimal hydrogen–oxygen molar ratio depending on the geometry of the burner was found to be at about 1.00–1.25 and the optimal precursor vapor feeding rate was somewhere between 350-400 mL/min. The average particle diameter of the best photocatalysts were found to be in the range of 50–70 nm, their specific surface area was between 20 and 28 m^2/g and they contained anatase in 80–95 wt% and the rest is rutile. These conditions provided optimal photocatalytic activity for the decomposition of phenol. When it is expressed in terms of the initial rate of photocatalytic phenol decomposition, our best photocatalysts exceeded the photocatalytic activity of P25 by a factor of 1.5, while their normalized activity (expressed in converted molecules in mol s^{-1} m^{-2} unit) was higher by a factor of almost 4. Our results prove, that bare (undoped) TiO_2 photocatalysts with photocatalytic activity significantly better than that of P25 can routinely be prepared and their performance optimized via the fine-tuning of the synthesis parameters employed.

Acknowledgements

KM thanks the Magyary Zoltán Foundation for the kind financial support. This work was financially supported by grants from the Hungarian National Office of Research and Technology (NKFP DA_THERM TECH_08_A4) and the Hungarian Research Foundation (OTKA, grant no. 67559, 78378 and 80193) and the bilateral Hungarian-Romanian TeT cooperation project (OMFB-00415/2008/RO-21/2007). Authors would like also to thank the opportunity provided by the Department of Colloid Chemistry at the University of Szeged, led by Professor Imre Dékány to have an access to a broad range of material characterization techniques.

References

[1] N. Balázs, K. Mogyorósi, D.F. Srankó, A. Pallagi, T. Alapi, A. Oszkó, A. Dombi, P. Sipos, Appl. Catal. B 84 (2008) 356–362.
[2] Z. Ambrus, K. Mogyorósi, Á. Szalai, T. Alapi, K. Demeter, A. Dombi, P. Sipos, Appl. Catal. A 340 (2008) 153–161.
[3] P. Calza, E. Pelizzetti, K. Mogyorósi, R. Kun, I. Dékány, Appl. Catal. B 72 (2007) 314–321.
[4] J. Ryu, W. Choi, Environ. Sci. Technol. 42 (2008) 294–300.
[5] K. Mogyorosi, A. Farkas, I. Dekany, I. Ilisz, A. Dombi, Environ. Sci. Technol. 36 (2002) 3618–3624.
[6] I. Ilisz, A. Dombi, K. Mogyorósi, A. Farkas, I. Dékány, Appl. Catal. B 39 (2002) 247–256.
[7] I. Ilisz, A. Dombi, K. Mogyorósi, I. Dékány, Colloids Surf. A 230 (2004) 89–97.
[8] M. Formenti, F. Juillet, P. Meriaudeau, S.J. Teichner, P. Vergnon, J. Colloid Interface Sci. 39 (1972) 79–89.
[9] V. Tiwari, J. Jiang, V. Sethi, P. Biswas, Appl. Catal. A 345 (2008) 241–246.
[10] G.L. Chiarello, E. Selli, L. Forni, Appl. Catal. B 84 (2008) 332–339.
[11] Y. Zhao, C. Li, X. Liu, F. Gu, H.L. Du, L. Shi, Appl. Catal. B 79 (2008) 208–215.
[12] K.K. Akurati, A. Vital, J.P. Dellemann, K. Michalow, T. Graule, D. Ferri, A. Baiker, Appl. Catal. B 79 (2008) 53–62.
[13] W.Y. Teoh, R. Amal, L. Mädler, S.E. Pratsinis, Catal. Today 120 (2007) 203–213.
[14] Y. Zhao, C. Li, X. Liu, F. Gu, J. Alloys Compd. 440 (2007) 281–286.
[15] R. Kavitha, S. Meghani, V. Jayaram, Mater. Sci. Eng. B 139 (2007) 134–140.
[16] K.K. Akurati, A. Vital, G. Fortunato, R. Hany, F. Nueesch, T. Graule, Solid State Sci. 9 (2007) 247–257.
[17] H. Park, B. Neppolian, H.S. Jie, J.P. Ahn, J.K. Park, M. Anpo, D.Y. Lee, Curr. Appl. Phys. 7 (2007) 118–123.
[18] W.Y. Teoh, L. Mädler, D. Beydoun, S.E. Pratsinis, R. Amal, Chem. Eng. Sci. 60 (2005) 5852–5861.
[19] R. Hong, Z. Ren, J. Ding, H. Li, Chem. Eng. J. (Amsterdam, Heth) 108 (2005) 203–212.
[20] C.B. Almquist, P. Biswas, J. Catal. 212 (2002) 145–156.
[21] J.R. McCormick, B. Zhao, S.A. Rykov, H. Wang, J.G. Chen, J. Phys. Chem. B 108 (2004) 17398–17402.
[22] P. Sunsap, D.J. Kim, K.S. Kim, Ind. Eng. Chem. Res. 47 (2008) 2308–2313.
[23] S. Kim, J.J. Gislason, R.W. Morton, X.Q. Pan, H.P. Sun, R.M. Laine, Chem. Mater. 16 (2004) 2336–2343.
[24] M.Z. Yu, J.Z. Lin, T.L. Chan, Chem. Eng. Sci. 63 (2008) 2317–2329.
[25] Y. Zhao, C. Li, X. Liu, F. Gu, H.L. Du, L. Shi, Mater. Chem. Phys. 107 (2008) 344–349.
[26] A. Teleki, R. Wengeler, L. Wengeler, H. Nirschl, S.E. Pratsinis, Powder Technol. 181 (2008) 292–300.
[27] Y. Zhao, C. Li, X. Liu, F. Gu, H. Jiang, W. Shao, L. Zhang, Y. He, Mater. Lett. 61 (2007) 79–83.
[28] B. Zhao, K. Uchikawa, J.R. McCormick, C.Y. Ni, J.G. Chen, H. Wang, Proc. Combust. Inst. 30 (2005) 2569–2576.
[29] K.K. Akurati, A. Vital, U.E. Klotz, B. Bommer, T. Graule, M. Winterer, Powder Technol. 165 (2006) 73–82.
[30] H.D. Jang, S.K. Kim, Mater. Res. Bull. 36 (2001) 627–637.
[31] G. Skandan, Y.-J. Chen, N. Glumac, B.H. Kea, Nanostruct. Mater. 11 (1999) 149–158.
[32] M. Aromaa, H. Keskinen, J.M. Mäkelä, Biomol. Eng. 24 (2007) 543–548.
[33] P.P. Ahonen, J. Joutsensaari, O. Richard, U. Tapper, D.P. Brown, J.K. Jokiniemi, E.I. Kauppinen, J. Aerosol Sci. 32 (2001) 615–630.
[34] I. Osama, Arabi-Katbi, Karsten Wegner, E. Sotiris, Pratsinis, Ann. Chim. Sci. Matér. 27 (2002) 37–46.
[35] A. Teleki, S.E. Pratsinis, K. Kalyanasundaram, P.I. Gouma, Sens. Actuators B 119 (2006) 683–690.
[36] H. Zhang, J.F. Banfield, J. Phys. Chem. B 104 (2000) 3481–3487.
[37] D.C. Hurum, A.G. Agrios, K.A. Gray, T. Rajh, M.C. Thurnauer, J. Phys. Chem. B 107 (2003) 4545–4549.
[38] D.C. Hurum, K.A. Gray, T. Rajh, M.C. Thurnauer, J. Phys. Chem. B 109 (2005) 977–980.
[39] A.K. Datye, G. Riegel, J.R. Bolton, M. Huang, M.R. Prairie, J. Solid State Chem. 115 (1995) 236–239.
[40] S.E. Pratsinis, Prog. Energy Combust. Sci. 24 (1998) 197–219.
[41] R. Strobel, A. Baiker, S.E. Pratsinis, Adv. Powder Technol. 17 (2006) 457–480.
[42] H.K. Kammler, S.E. Pratsinis, P.W. Morrison Jr., B. Hemmerling, Combust. Flame 128 (2002) 369–381.
[43] O.I. Arabi-Katbi, S.E. Pratsinis, P.W. Morrison Jr., C.M. Megaridis, Combust. Flame 124 (2001) 560–572.
[44] H. Wang, Y. Wu, B.-Q. Xu, Appl. Catal. B 59 (2005) 139–146.
[45] T. Moritz, J. Reiss, K. Diesner, D. Su, A. Chemseddine, J. Phys. Chem. B 101 (1997) 8052–8053.
[46] B. Koo, J. Park, Y. Kim, S.-H. Choi, Y. -E- Sung, T. Hyeon, J. Phys. Chem. B 110 (2006) 24318–24323.
[47] K. Chhor, J.F. Bocquet, C. Colbeau-Justin, Mater. Chem. Phys. 86 (2004) 123–131.
[48] U. Diebold, Surf. Sci. Rep. 48 (2003) 53–229.